Polarization-tuneable excitonic spectral features in the optoelectronic response of atomically thin ReS_2

To cite this article: Daniel Vaquero *et al* 2024 *2D Mater.* **11** 015011

2D Materials

OPEN ACCESS

RECEIVED
21 June 2023

REVISED
6 October 2023

ACCEPTED FOR PUBLICATION
16 October 2023

PUBLISHED
13 November 2023

PAPER

Polarization-tuneable excitonic spectral features in the optoelectronic response of atomically thin ReS_2

Daniel Vaquero[1,5], Olga Arroyo-Gascón[2,3,5], Juan Salvador-Sánchez[1,5], Pedro L Alcázar-Ruano[3], Enrique Diez[1], Ana Perez-Rodríguez[1], Julián D Correa[4], Francisco Dominguez-Adame[3], Leonor Chico[3] and Jorge Quereda[3,*]

[1] Nanotechnology Group, USAL–Nanolab, Universidad de Salamanca, E-37008 Salamanca, Spain
[2] Instituto de Ciencia de Materiales de Madrid, CSIC, E-28049 Madrid, Spain
[3] Departamento de Física de Materiales, GISC, Universidad Complutense de Madrid, E-28040 Madrid, Spain
[4] Facultad de Ciencias Básicas, Universidad de Medellín, Medellín, Colombia
[5] These authors contributed equally to the work.
[*] Author to whom any correspondence should be addressed

E-mail: jorquere@ucm.es

Keywords: optoelectronics, exciton, ReS_2, polarization-dependent, photocurrent spectroscopy

Supplementary material for this article is available online

Abstract

The low crystal symmetry of rhenium disulphide (ReS_2) leads to the emergence of dichroic optical and optoelectronic response, absent in other layered transition metal dichalcogenides, which could be exploited for device applications requiring polarization resolution. To date, spectroscopy studies on the optical response of ReS_2 have relied almost exclusively in characterization techniques involving optical detection, such as photoluminescence, absorbance, or reflectance spectroscopy. However, to realize the full potential of this material, it is necessary to develop knowledge on its optoelectronic response with spectral resolution. In this work, we study the polarization-dependent photocurrent spectra of few-layer ReS_2 photodetectors, both in room conditions and at cryogenic temperature. Our spectral measurements reveal two main exciton lines at energies matching those reported for optical spectroscopy measurements, as well as their excited states. Moreover, we also observe an additional exciton-like spectral feature with a photoresponse intensity comparable to the two main exciton lines. We attribute this feature, not observed in earlier photoluminescence measurements, to a non-radiative exciton transition. The intensities of the three main exciton features, as well as their excited states, modulate with linear polarization of light, each one acquiring maximal strength at a different polarization angle. We have performed first-principles exciton calculations employing the Bethe-Salpeter formalism, which corroborate our experimental findings. Our results bring new perspectives for the development of ReS_2-based nanodevices.

1. Introduction

Layered transition metal dichalcogenides (TMDs) have attracted enormous attention in the last decade due to their great potential for optics and optoelectronics [1, 2]. The effect of quantum confinement in these materials, combined with a reduced electrostatic screening, results in long-lived excitonic states, [3] which dominate their optical response. Further, TMDs also present valley-dependent optical selection rules, which allow to selectively generate excitons in a given valley simply by tuning the polarization of incident light [4, 5].

To date, the most studied TMDs are those containing a group VI transition metal, i.e., MoS_2, $MoSe_2$, WS_2 and WSe_2, mainly because they present excitonic transitions with remarkably strong oscillator strengths and narrow bandwidths. However, in the last years, Re-based TMDs (ReS_2 and $ReSe_2$) have gained increasing attention. These materials also present strong exciton transitions and, differently from group VI crystals, their reduced crystal

symmetry leads to optical anisotropy [6–8]. Excitonic features in the photoluminescence and differential reflectance spectra of ReS_2 present linear dichroism, with different exciton transitions acquiring their maximal intensity for different polarizations of light.

While the band structure and optical spectrum of atomically thin ReS_2 have been studied by several research groups, there are still many open questions regarding its fundamental properties. For example, different works disagree on the nature of the fundamental bandgap (either direct or indirect), as well as in the labeling of the different excitonic transitions. Discussion has also arisen regarding the actual crystalline structure of ReS_2, with two different growth directions reported experimentally [9, 10], both with very similar total energies [11]. Additionally, ReS_2 multilayers have been lately found to present two stable stacking orders at room temperature [12, 13], with substantially different optical properties. Thus, the apparently contradictory results reported in the literature for the bandgap and optical response of ReS_2 crystals may be related to the existence of multiple stable crystalline structures, each with different band dispersions. The optoelectronic properties of ReS_2 are also not fully characterized yet. In particular, current literature lacks detailed information on the spectral dependence of photoresponse in ReS_2-based devices, of crucial importance for several technological applications.

In this work we focus on the optoelectronic response of few-layer ReS_2 phototransistors. The strong Coulomb interaction and the low symmetry of the crystalline structure of ReS_2 have a significant impact on the optical response of the photodetectors, which is dominated by exciton transitions even at moderate temperature. By resorting to low-temperature photocurrent spectroscopy [14, 15], we identify three main excitonic features, whose intensities modulate as a function of the polarization of incident light. To uncover the origin of the excitonic features observed in the spectra, we have also performed density functional theory (DFT) first-principles calculations to obtain the band structure of ReS_2. From this band structure, exciton absorption spectra have been obtained, allowing us to identify the excitonic origin of the various features observed in the optical spectra.

2. Results

2.1. Device and measurement geometry

The crystal structure of monolayer ReS_2 presents a distorted 1T structure [16], where two nonequivalent perpendicular directions are present, either parallel or perpendicular to the *b* crystalline axis. In multilayer crystals, the stacking between layers presents two different stable configurations, named in the literature as AA and AB stacking [12, 13]. For AA-stacked crystals the successive layers are positioned directly on top of each other, while for AB stacking consecutive layers are shifted by roughly 2.5 Å across the *a* crystalline axis. The orientation of the ReS_2 crystalline axes, as well as the stacking configuration can be revealed by polarization-resolved Raman spectroscopy (see supplementary note 1) and photoluminescence spectroscopy (supplementary note 2).

In order to explore the optoelectronic properties of few-layer ReS_2, we fabricate field-effect phototransistors using mechanically exfoliated few-layer ReS_2 crystals as the semiconductor channel. Figure 1(a) shows a microscope image of a typical ReS_2 device, fabricated with an AB-stacked ReS_2 crystal. Detailed discussion on the device fabrication and electrical characterization are provided supplementary notes 3 and 4, respectively.

To characterize the photoresponse of ReS_2 we expose the whole area of the device to homogeneous monochromatic light and measure the drain–source current at fixed gate and drain–source voltages. We define the photocurrent I_{PC} as the difference between the drain–source current measured under illumination and in the dark (see figure 1(b)).

We find that the device photoresponse is relatively fast, with response times in the order of 1 ms (see supplementary note 5). It is also worth remarking that we did not observe any long-lasting photodoping effects, even when they are frequently found in 2D material-based devices.

2.2. Photocurrent spectroscopy measurements

Next, we explore the exciton physics of few-layer ReS_2 by low-temperature photocurrent spectroscopy. Unless otherwise stated, all the measurements presented here are acquired at 7 K using the AB-stacked ReS_2 device shown in figure 1(a). Room-temperature measurements and measurements for an AA-stacked crystal are provided in supplementary notes 6 and 7, respectively. We use a lock-in amplifier to register the photocurrent in the device while continuously switching the illumination on and off at a fixed frequency of 31.81 Hz. The photoresponsivity spectra are obtained by repeating this measurement while scanning the illumination wavelength. Further details regarding the procedure for spectral acquisition can be found in supplementary note 8. Figure 1(c) shows a typical ReS_2 photoresponsivity spectrum, acquired for light polarization perpendicular to the *b* crystalline axis. The experimentally measured photoresponse presents numerous exciton-like features in the energy range from 1.45 eV to 1.7 eV, in good agreement with the spectral features reported in literature for low-temperature photoluminescence spectroscopy in ReS_2 [17, 18].

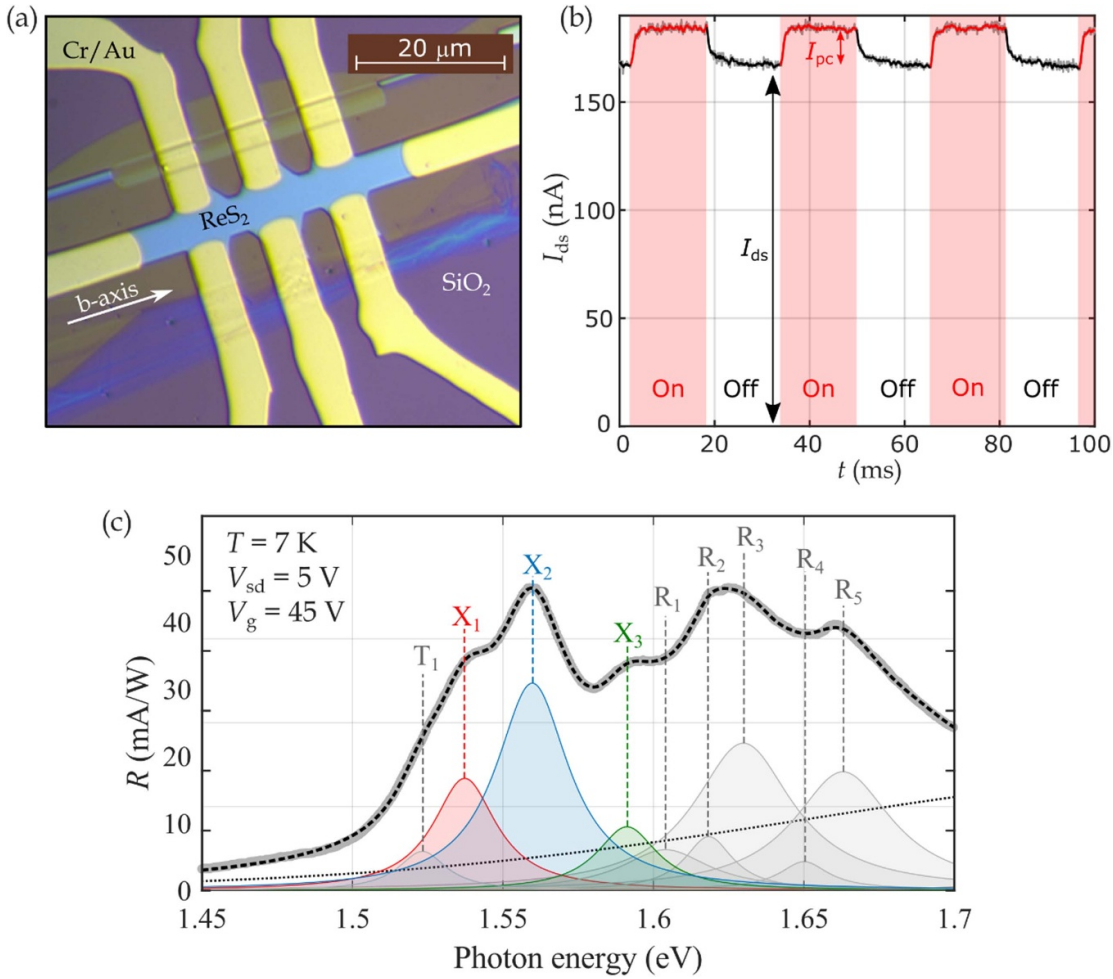

Figure 1. Optoelectronic response of the device. (a) Optical microscopy image of the ReS_2 photodetector (b) source-drain current of the photodetector at $V_{sd} = 5$ V and $V_g = 45$ V. When the light excitation ($\lambda = 620$ nm) is turned on, the drain–source current increases by I_{PC}. (c) Photocurrent spectrum at $V_{sd} = 5$ V, $V_g = 45$ V and a power density of 500 W m^{-2}. The spectrum is acquired for light polarization perpendicular to the *b*-axis of the ReS_2 crystal. The grey curve is the experimentally measured spectrum. The dashed black curve is a least square fit to a multi-Lorentzian function plus a smooth background, which accounts for direct band-to-band absorption. The individual Lorentzian peaks are also shown in the figure.

Our spectra present two prominent peaks, X_1 and X_2, at roughly 1.54 and 1.56 eV (highlighted in figure 1(c) in red and blue, respectively). These two spectral features have also been observed in earlier literature by low-temperature PL, PLE and micro-reflectance spectroscopy [7, 17, 19]. *Ab-initio* calculations have shown that ReS_2 has two direct bandgap minima with very similar energies, occurring at the K_1 and Z points of the reciprocal lattice [20]. Thus, X_1 and X_2 are usually attributed to exciton absorption at K_1 and Z, respectively [21]. In our spectra, we also observe a smaller satellite peak at 1.525 eV, 14 meV below X_1, which we attribute to the trion state T_1 associated with X_1. A third, less prominent peak is also observed at 1.588 eV. We believe that this feature, not reported in earlier literature, may be related with a higher-energy exciton transition, which we label as X_3 (further discussed below). Finally, a cluster of exciton-like peaks appears at energies between 1.6 and 1.7 eV, which we attribute to the Rydberg series of excited states of the main excitons. These secondary peaks, as well as the main excitonic features, are also present in our DFT simulations of the absorption spectrum of ReS_2. The energies of the excitonic peaks obtained theoretically are in good agreement with our experimental findings, as explained in the section 3.

The dashed line in figure 3 shows a fitting of the experimental spectrum to a multi-Lorentzian function. The function includes individual Lorentzian peaks to account for the T_1, X_1, X_2 and X_3 peaks, as well as five additional peaks (labeled here as R_1–R_5) to account for the most prominent spectral features between 1.6 and 1.7 eV. It must be noted that, since peaks R_1–R_5 are not fully resolved in our spectra, it is possible that a larger number of optical transitions are present at this energy range. Thus, more than one optical process may be contributing to photoresponse for each of the assigned peaks. In

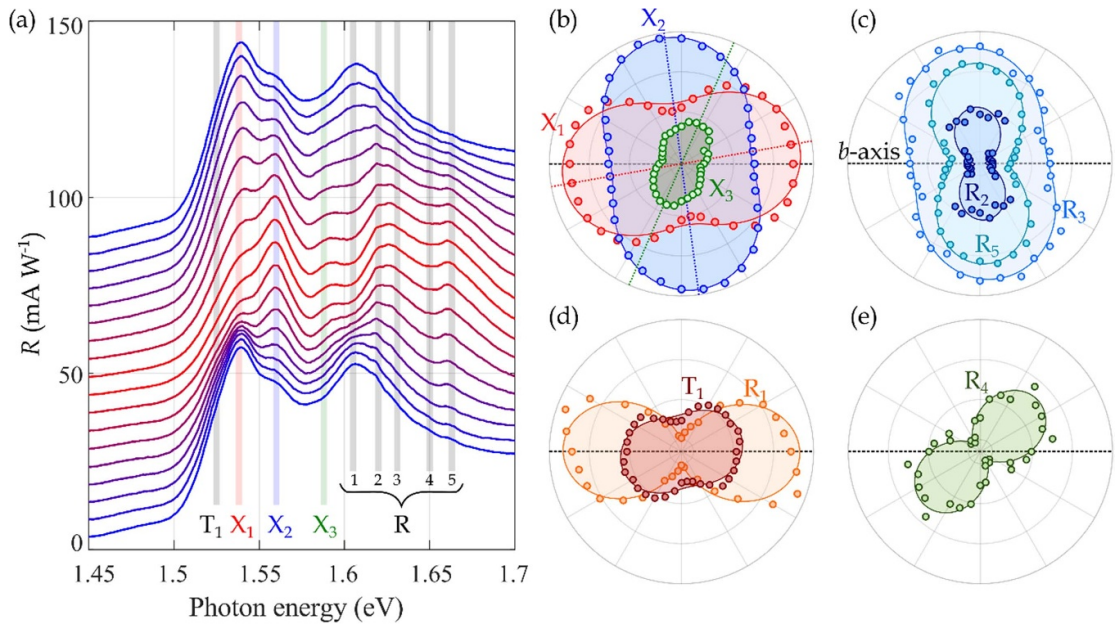

Figure 2. (a) Photocurrent spectra acquired for different angles of light polarization, from 0 to 170° relative to the *b* crystalline axis, with $V_{sd} = 5$ V, $V_g = 45$ V and a power density of 500 W m^{-2}. Consecutive spectra have been shifted vertically in steps of 5 mA W^{-1} for easier visualization. (b)–(e) Polar plots showing the modulation of the different spectral features as a function of the polarization direction, extracted from fittings to multi-Lorentzian curves, as the one shown in figure 1(c).

addition to the different Lorentzian peaks, our fitting function also includes a Fermi–Dirac distribution function centered at 1.7 eV (shown as a dotted line in the figure) to account for the effect of direct interband transitions.

2.3. Polarization dependence of photocurrent spectra

In order to achieve a clearer picture of the exciton physics in ReS_2, we next characterize the dependence of photocurrent spectra on the polarization of the optical excitation. Figure 2(a) shows a series of photocurrent spectra acquired for different angles of polarization. All the spectral features described above are strongly affected by the polarization direction. Figure 2(b) shows the intensity of the three main exciton lines (X_{1-3}) as a function of the direction of polarization. Exciton X_1 becomes maximal when light polarization is at 10° relative to the *b* axis of the crystal, while X_2 maximizes at 95° polarization, almost perpendicular to X_1. The spectral feature at 1.525 eV follows the same polarization dependence of X_1, supporting its labeling as the trion state T_1. Finally, exciton X_3 becomes maximal for a polarization angle of 65°. The fact that the polarization dependence of X_3 is different from those of X_1 and X_2 supports the idea that X_3 does not correspond to an excited state of neither X_1 nor X_2, but it is indeed originated from an exciton transition at a different point of the reciprocal lattice. As shown in panels *c* to *e* of figure 2, the remaining spectral features with energies above 1.6 eV follow the same polarization dependence as one of the three main exciton peaks, suggesting that they are originated by excited states of either of the main excitons. In particular, we find that R_1 emulates the same polarization dependence of X_1, while R_2, R_3 and R_5 emulate the dependence of X_2. R_4 becomes maximal at an angle of 40°, and probably contains contributions of excited states from both X_1 and X_3.

Our results are highly compatible with earlier reports on low-temperature photoluminescence spectroscopy for few-layer ReS_2. Indeed, said reports also revealed the X_1 and X_2 spectral features at very similar energies to the ones obtained here, as well as higher-energy features corresponding to excited states of these two excitons. However, the spectral feature labeled here as X_3 is not observed in earlier reported photoluminescence spectra. Thus, we believe that this feature may correspond to a non-radiative exciton level (further discussed below).

2.4. Role of in-plane electric field on the photocurrent spectra

We now turn our attention to the effect of the drain–source voltage in the photocurrent spectra. Since excitons are charge-neutral, they need to dissociate into free electron-hole pairs in order to contribute to photoresponse. In typical 2D phototransistors, this exciton dissociation process mainly takes place in the vicinity of the electrodes, where the presence of Schottky barriers results in very strong in-plane

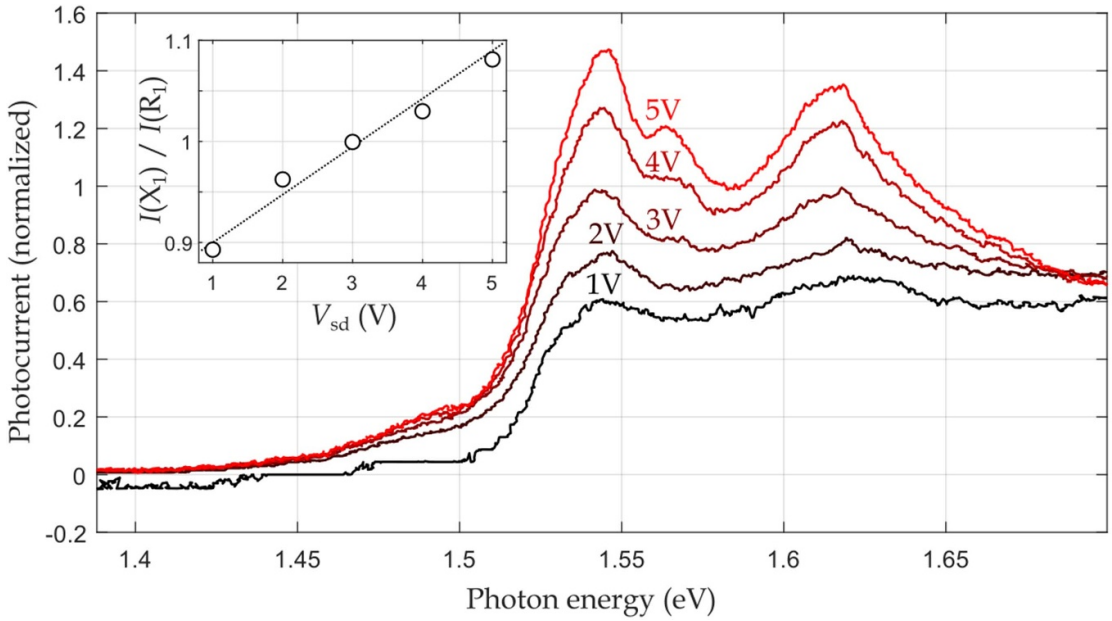

Figure 3. Photocurrent spectra acquired for different V_{sd}, ranging between 1 V and 5 V, for $V_g = 45$ V, a power density of 500 W m^{-2}, and light polarization parallel to the *b*-axis of the ReS_2 crystal. To facilitate comparison between the different spectra, they have been normalized to the value of photoresponse at 1.9 eV. The inset shows the ratio between the photocurrent at 1.54 and 1.62 eV, on resonance with peaks X_1 and R_1, respectively. As V_{sd} is increased, this ratio becomes progressively larger.

electric fields [22]. Figure 3 shows five individual photocurrent spectra, acquired at different source–drain voltages, ranging from 1 V to 5 V. To facilitate comparison, the five spectra have been normalized to the value of the photocurrent at 1.9 eV, where photoresponse should be mainly caused by direct interband absorption. As expected, when we increase the source–drain voltage (and therefore the in-plane electric field) exciton dissociation processes become stronger, and the excitonic spectral features become progressively more prominent relative to the smooth background caused by interband transitions. This effect is particularly noticeable for the X_2 peak, which is barely visible at low V_{sd} due to the presence of more prominent spectral features in its vicinity, but becomes clearly resolved at $V_{sd} = 5$ V. Furthermore, we observe that the relative intensity of the excitonic features is also affected by V_{sd}, with the $X_{1–3}$ peaks becoming more prominent as V_{sd} increases, relative to the $R_{1–5}$ peaks. This was also expected, as the excited Rydberg states have weaker binding energies compared to the fundamental states and, therefore, exciton dissociation for these states may occur at weaker electric fields.

2.5. Gate voltage dependence of the photocurrent spectra

Finally, we characterize the gate voltage dependence of the photocurrent spectra. Figure 4(a) shows a set of photocurrent spectra acquired at different gate voltages (V_g), ranging from 24 to 50 V, for polarization parallel to the *b*-axis of the ReS_2 crystal. As expected for photogating, the overall photoresponse of the device decreases as V_g is lowered. Thus, to facilitate comparison of spectral features, each spectrum has been normalized to the value of photocurrent at 1.8 eV, far away from the exciton transitions. Three main effects can be observed here: firstly, the overall intensity of excitonic peaks relative to the smooth background increases with the gate voltage, suggesting that exciton dissociation processes become more efficient at higher gate voltages, possibly due to an increased scattering with conduction-band electrons.

Secondly, the relative weight of the higher-energy peaks labeled as R_1–R_5 modulates in a highly nontrivial manner. While we do not fully understand the origin of this complex gate modulation of Rydberg states, a similar effect has been also observed in the photocurrent spectra of monolayer MoS_2 [14, 15].

Lastly, we find that the relative intensity of the X_1 and T_1 peaks is also affected by the gate voltage. Figure 4(b) shows the ratio between the intensities of T_1 and X_1 as a function of V_g. When the V_g is increased, the spectral weight is transferred from the neutral exciton state to the trion state, and the ratio I_{T1}/I_{X1} increases monotonically. This modulation suggests that T_1 corresponds to a negatively charged trion state.

3. Discussion

As discussed in the introduction, both experimental and theoretical works on ReS_2 span a variety of results, sometimes contradictory. The first discrepancy

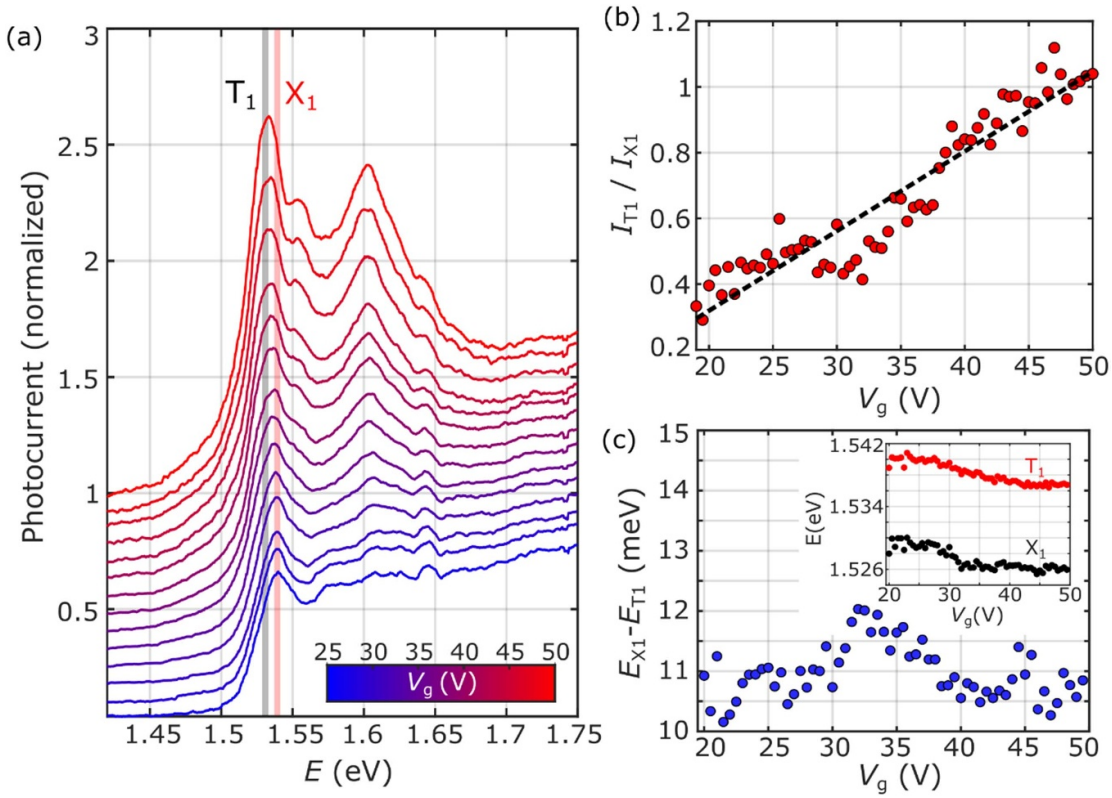

Figure 4. Gate dependence of photocurrent spectra. (a) Photocurrent spectra acquired for different V_g, ranging between 24 V and 50 V, for $V_{sd} = 5$ V, a power density of 500 W m^{-2}, and light polarization parallel to the *b*-axis of the ReS_2 crystal. To facilitate comparison between the different spectra, they have been shifted vertically relative to each other, and the intensity of each individual spectrum has been normalized to the value of photoresponse at 1.8 eV. (b) Ratio between the intensities of the X_1 and T_1 spectral peaks as a function of V_g. (c) Energy difference between the X_1 and T_1 spectral peaks, extracted from multi-Lorentzian fittings of the spectral profiles, as a function of V_g. The inset shows the individual energy values obtained for X_1 and T_1.

arises from the report of two possible triclinic structures, either grown along the *c*-axis [9], or along the *a*-axis [10]. These two different structures present slight (but not negligible) differences as to their bands and the direct or indirect character of their gaps, which have called the attention of several research groups. [11, 23–25] But since the difference in total energy is very small, [11] these results are compatible with the fact that both structures can be grown depending on the substrate and experimental conditions. In any case, the theoretically reported bulk gaps range from 1.32 eV by Gadde *et al* [23] to 1.6 eV by Echeverry and Gerber [26] for the *c*-axis and *a*-axis structure respectively, but at different points of the Brillouin zone. In fact, Gadde *et al* have performed a numerical comparison between the two crystalline structures and report an indirect gap for the *a*-axis structure of 1.49 eV [23]. Interestingly, other authors have pointed out that a smaller gap, from 1.2 eV to 1.29 eV, can be obtained if the whole band structure is studied, and not only along the high-symmetry paths and edges of the Brillouin zone, as it is customarily done [24]. This observation is relevant given the low symmetry of this material, and it has also been reported in other low-symmetry systems [27]. Nevertheless, since many-body effects are neglected in most calculations, it is expected that not only the gap character may change from direct to indirect if these effects are included, but also an increase of its value and a flattening of the bands.

Since our experimental samples follow the *a*-aligned crystal structure, we have performed our DFT simulations employing such geometry. Several exchange-correlation functionals and methods were tested, yielding indirect gaps between 1.24 eV and 1.26 eV, in agreement with the former works discussed above, except for the TB09 functional which results in a 1.425 eV gap, in a similar way to other meta-generalized gradient approximation (GGA) functionals (see section 4). In supplementary note 9 we present the band structure of ReS_2 computed with the Perdew-Burke-Ernzerhof (PBE) functional. A detailed comparison of the exciton absorption energies obtained via the Bethe–Salpeter equation for all tested functionals is gathered in table 1.

Due to the low symmetry of ReS_2, the number of atoms in our DFT unit cell makes this material a good candidate for meta-GGA calculations. Since a dynamically screened approximation (GW) calculations result in an overall uniform shift of the bands,

Table 1. Exciton absorption energies of the experimental data fit (column 2) and DFT results for several functionals (columns 3–6). The last two columns gather other theoretical works, where only the first peaks were discussed. The feature at 1.40 eV is described in the literature as an indirect transition [13, 26]. All units are in eV.

Label	Exp.	PBE	vdW-DF	vdW-DF2	TB09	Reference [13]	Reference [26]
—	—	—	—	—	—	1.40	1.40
—	—	—	—	—	—	1.46	—
T_1	1.524	—	1.514	1.50	1.471	1.50	1.51
X_1	1.537	1.538	1.543	1.535	1.535	—	—
X_2	1.558	1.562	—	—	1.575	1.56	1.56
X_3	1.590	—	1.602	1.590	1.592	—	—
R_1	1.607	—	—	1.604	1.60	—	—
R_2	1.619	1.616	1.621	1.614	1.621	—	—
R_3	1.631	1.629	1.628	1.633	1.636	—	—
R_4	1.649	1.645	—	1.644	1.641	—	—
R_5	1.660	1.654	1.662	1.656	1.665	—	—

different scissor shifts are performed for each column on table 1, so that the gap of each functional matches the GW one [26], as detailed in the supplementary information. We find a general agreement between theoretical and experimental data for all functionals. The TB09 calculation reproduces successfully all the main excitonic features, including the newly reported transition at around 1.59 eV, labeled X_3 in the former section. However, the X_2 feature is best described by the PBE functional. Thus, we conclude PBE and TB09 yield the most precise results among all functionals studied, being the TB09 calculation the excelling one, with a thorough description of all experimental peaks.

In all, the spectral characterization of ReS_2 photoresponse reported here shines new light on the polarization-dependent optoelectronic response of excitons on ReS_2. In particular, the observation of a novel exciton transition in our photocurrent spectra, not reported in earlier literature for optical spectroscopy measurements opens new possibilities for studying and exploiting excitonic phenomena in ReS_2-based optoelectronic devices. However, further work is needed to fully clarify the origin and properties of this newly observed excitonic feature.

4. Methods

Photocurrent spectral acquisition—The sample is placed inside a closed cycle cryostat at $T = 7$ K with an optical access and exposed to laser illumination. The light source is a supercontinuum (white) laser (SuperK Compact), and the excitation wavelength is selected using a monochromator (Oriel MS257 with 1200 lines mm^{-1} diffraction grid). This allows to scan the visible and NIR spectral range, roughly from 450 nm to 1000 nm. The polarization of the light is selected using a linear polarizer and a half-waveplate. Electrical measurements are performed with a doubled channel sourcemeter (Keithley 2614b). For AC optoelectronic measurements, the optical excitation is modulated by a mechanical chopper and the photoresponse of the device is registered using a lock-in amplifier (Stanford Research SR830).

Raman and photoluminescence spectroscopy—For Raman and photoluminescence spectroscopy measurements we use a Horiba LabRam HR micro-Raman spectrometer with a 100× objective under 532 nm laser excitation in normal incidence on the sample. Raman polarization-resolved measurements are performed rotating the sample while the excitation and detected light have the same polarization. Photoluminescence-resolved measurements are performed fixing the sample position and changing the polarization angle of the collected light using a linear polarizer.

First principles simulations—DFT simulations were mainly performed using the GPAW code [28–30] with a plane wave energy cutoff of 500 eV. A $10 \times 10 \times 10$ Monkhorst–Pack grid was used for the k-space sampling, and we considered structural relaxations until forces on the atoms were below 0.001 eV $Å^{-1}$. A full Brillouin zone analysis and comparison with former works [11, 24] yields slightly more precise band gaps for the unrelaxed geometry, which also provides a more direct comparison with our experimental samples.

Several exchange-correlation functionals were tested under the GGA. In particular, the PBE parametrization and van der Waals corrections under the vdWDF and vdW-DF2 approximations were used [31]. Additionally, the meta-GGA Tran–Baha modified Becke–Johnson (TB09) functional is considered in order to render a more accurate description of the band gap [31]. The gaps for the PBE and van der Waals functionals range from 1.243 to 1.263 eV, whereas the TB09 functional gives a 1.425 eV gap. Spin–orbit coupling was shown not to have an impact in the location of direct transitions since band splittings are forbidden by inversion symmetry (see figure S11 in supplementary information). Moreover, equivalent band structure calculations were performed

resorting to the SIESTA code [32, 33], yielding a good agreement between both methods.

As for the absorbance spectrum, the Bethe–Salpeter equation as implemented in GPAW was employed. A 9 × 9 × 9 Monkhorst–Pack mesh was used for these calculations. 5 valence and 5 conduction bands were considered, as well as an energy cutoff of 100 eV. For the sake of comparison, this calculation was performed for the PBE, vdW-DF, vdW-DF2 and TB09, as shown in table 1 in the main text. A scissor shift is applied to each calculation in order to reproduce the results one would obtain performing BSE over a GW method. Specifically, the applied shift amounts to 0.375, 0.349, 0.339 and 0.167 eV for the PBE, vdW-DF, vdW-DF2 and TB09 functionals, respectively.

Data availability statement

All data that support the findings of this study are included within the article (and any supplementary files).

Acknowledgments

We thank Mercedes Velázquez for her help with the photoluminescence and Raman characterization setup. We thank Yahya M Meziani and Adrián Martín-Ramos for their assistance on the development of the photocurrent spectroscopy measurement setup. We thank Vito Clericò for his assistance on the device fabrication process. We thankfully acknowledge the computer resources at FinisTerrae III and the technical support provided by Centro de Supercomputación de Galicia, CESGA (FI-2023-1-0038).

Author contributions

J Q conceived and supervised the research. D V-M, J S-S, A P-R and P L A-R were involved in the fabrication and electrical characterization of ReS_2 phototransistors. D V-M and A P-R carried out the electronic, optoelectronic, and spectral measurements and data analysis. O A-G, J D C, L C and F D-A performed the theoretical analysis. The article was written through contribution of all the authors, coordinated by J Q. All authors have given approval to the final version of the manuscript.

Funding sources

We acknowledge financial support from the Agencia Estatal de Investigación of Spain (Grants PID2022-136285NB, PID2019-106820RB, RTI2018-097180-B-100, and PGC2018-097018-B-I00). We acknowledge financial support by Comunidad de Madrid through the (MAD2D-CM)-UCM5 Project. We acknowledge financial support by Junta de Castilla y León (Grants SA256P18 and SA121P20), including funding by ERDF/FEDER. J Q acknowledges the financial support received from the Marie Skłodowska Curie-COFUND program under the Horizon 2020 research and innovation initiative of the European Union, within the framework of the UNA4CAREER program (Grant Agreement 4129252). D V-M acknowledges financial support from the Spanish Ministry of Universities (PhD contract FPU19/04224). O A-G acknowledges the support of Grant PRE2019-088874 funded by MCIN/AEI/10.13039/501100011033 and by 'ESF Investing in your future'. A P-R acknowledges the financial support received from the Marie Skłodowska Curie-COFUND program under the Horizon 2020 research and innovation initiative of the European Union, within the framework of the USAL4Excellence program (Grant Agreement 101034371). J S-S acknowledges financial support from the Consejería de Educación, Junta de Castilla y León (EDU/875/2021), and ERDF/FEDER.

ORCID iDs

Pedro L Alcázar-Ruano https://orcid.org/0000-0002-5350-9252
Enrique Diez https://orcid.org/0000-0001-7964-4148
Leonor Chico https://orcid.org/0000-0002-7131-1266
Jorge Quereda https://orcid.org/0000-0003-1329-5242

References

[1] Manzeli S, Ovchinnikov D, Pasquier D, Yazyev O V and Kis A 2017 2D transition metal dichalcogenides *Nat. Rev. Mater.* **2** 1–15
[2] Splendiani A, Sun L, Zhang Y, Li T, Kim J, Chim C-Y, Galli G and Wang F 2010 Emerging photoluminescence in monolayer MoS_2 *Nano Lett.* **10** 1271–5
[3] Mak K F, He K, Lee C, Lee G H, Hone J, Heinz T F and Shan J 2013 Tightly bound trions in monolayer MoS_2 *Nat. Mater.* **12** 207–11
[4] Macneill D, Heikes C, Mak K F, Anderson Z, Kormányos A, Zólyomi V, Park J and Ralph D C 2015 Breaking of valley degeneracy by magnetic field in monolayer $MoSe_2$ *Phys. Rev. Lett.* **114** 1–13
[5] Liu Y, Gao Y, Zhang S, He J, Yu J and Liu Z 2019 Valleytronics in transition metal dichalcogenides materials *Nano Res.* **12** 2695–711
[6] Chenet D A, Aslan B, Huang P Y, Fan C, van der Zande A M, Heinz T F and Hone J C 2015 In-plane anisotropy in mono- and few-layer ReS_2 probed by Raman spectroscopy and scanning transmission electron microscopy *Nano Lett.* **15** 5667–72
[7] Wang J *et al* 2020 Polarized light-emitting diodes based on anisotropic excitons in few-layer ReS_2 *Adv. Mater.* **32** 1–7
[8] Aslan O B, Chenet D A, Van Der Zande A M, Hone J C and Heinz T F 2016 Linearly polarized excitons in single- and few-layer ReS_2 crystals *ACS Photonics* **3** 96–101

[9] Lamfers H J, Meetsma A, Wiegers G A and De Boer J L 1996 The crystal structure of some rhenium and technetium dichalcogenides *J. Alloys Compd.* **241** 34–39
[10] Murray H H, Kelly S P, Chianelli R R and Day C S 1994 Structure of rhenium disulfide *Inorg. Chem.* **33** 4418–20
[11] Ibáñez-Insa J, Woźniak T, Oliva R, Popescu C, Hernández S and López-Vidrier J 2021 Structural and high-pressure properties of rheniite (ReS_2) and (Re,Mo)S_2 *Minerals* **11** 207
[12] Zhou Y *et al* 2020 Stacking-order-driven optical properties and carrier dynamics in ReS_2 *Adv. Mater.* **32** 1908311
[13] Zhou Y, Maity N, Lin J F, Singh A K and Wang Y 2021 Nonlinear optical absorption of ReS_2 driven by stacking order *ACS Photonics* **8** 405–11
[14] Vaquero D, Clericò V, Salvador-Sánchez J, Martín-Ramos A, Díaz E, Domínguez-Adame F, Meziani Y M, Diez E and Quereda J 2020 Excitons, trions and Rydberg states in monolayer MoS_2 revealed by low-temperature photocurrent spectroscopy *Commun. Phys.* **3** 194
[15] Vaquero D, Salvador-Sánchez J, Clericò V, Diez E and Quereda J 2022 The low-temperature photocurrent spectrum of monolayer $MoSe_2$: excitonic features and gate voltage dependence *Nanomaterials* **12** 322
[16] Wilson J A and Yoffe A D 1969 The transition metal dichalcogenides discussion and interpretation of the observed optical, electrical and structural properties *Adv. Phys.* **18** 193–335
[17] Ho C H and Liu Z Z 2019 Complete-series excitonic dipole emissions in few layer ReS_2 and $ReSe_2$ observed by polarized photoluminescence spectroscopy *Nano Energy* **56** 641–50
[18] Jadczak J, Kutrowska-Girzycka J, Smoleński T, Kossacki P, Huang Y S and Bryja L 2019 Exciton binding energy and hydrogenic Rydberg series in layered ReS_2 *Sci. Rep.* **9** 1–9
[19] Gogna R, Zhang L and Deng H 2020 Self-hybridized, polarized polaritons in ReS_2 crystals *ACS Photonics* **7** 3328–32
[20] Oliva R, Laurien M, Dybala F, Kopaczek J, Qin Y, Tongay S, Rubel O and Kudrawiec R 2019 Pressure dependence of direct optical transitions in ReS_2 and $ReSe_2$ *npj 2D Mater. Appl.* **3** 20
[21] Dhara A, Chakrabarty D, Das P, Pattanayak A K, Paul S, Mukherjee S and Dhara S 2020 Additional excitonic features and momentum-dark states in ReS_2 *Phys. Rev.* B **102** 161404(R)
[22] Ubrig N, Jo S, Philippi M, Costanzo D, Berger H, Kuzmenko A B and Morpurgo A F 2017 Microscopic origin of the valley Hall effect in transition metal dichalcogenides revealed by wavelength-dependent mapping *Nano Lett.* **17** 5719–25
[23] Gadde J R *et al* 2021 Two-dimensional ReS_2: solution to the unresolved queries on its structure and inter-layer coupling leading to potential optical applications *Phys. Rev. Mater.* **5** 054006
[24] Wang P, Wang Y, Qu J, Zhu Q, Yang W, Zhu J, Wang L, Zhang W, He D and Zhao Y 2018 Pressure-induced structural and electronic transitions, metallization, and enhanced visible-light responsiveness in layered rhenium disulphide *Phys. Rev.* B **97** 235202
[25] Ho C, Huang Y, Tiong K and Liao P C 1998 Absorption-edge anisotropy in ReS_2 and $ReSe_2$ layered semiconductors *Phys. Rev.* B **58** 16130
[26] Echeverry J P and Gerber I C 2018 Theoretical investigations of the anisotropic optical properties of distorted 1T ReS_2 and $ReSe_2$ monolayers, bilayers, and in the bulk limit *Phys. Rev.* B **97** 075123
[27] Bravo S, Correa J, Chico L and Pacheco M 2018 Tight-binding model for opto-electronic properties of penta-graphene nanostructures *Sci. Rep.* **8** 1–10
[28] Mortensen J J, Hansen L B and Jacobsen K W 2005 Real-space grid implementation of the projector augmented wave method *Phys. Rev.* B **71** 035109
[29] Enkovaara J *et al* 2010 Electronic structure calculations with GPAW: a real-space implementation of the projector augmented-wave method *J. Phys.: Condens. Matter* **22** 253202
[30] Hjorth Larsen A *et al* 2017 The atomic simulation environment-a Python library for working with atoms *J. Phys.: Condens. Matter* **29** 273002
[31] Lehtola S, Steigemann C, Oliveira M J T and Marques M A L 2018 Recent developments in libxc—A comprehensive library of functionals for density functional theory *SoftwareX* **7** 1–5
[32] Soler J M *et al* 2002 The SIESTA method for ab initio order-N materials simulation *J. Phys.: Condens. Matter* **14** 2745
[33] García A *et al* 2020 Siesta: recent developments and applications *J. Chem. Phys.* **152** 204108